

Coulomb-Nuclear Interference in Polarized pA Scattering

Boris Kopeliovich ^{1,*}, Michal Krelina ² and Irina Potashnikova ¹

¹ Universidad Técnica Federico Santa María, Avenida España 1680, 2390123 Valparaíso, Chile; irina.potashnikova@usm.cl

² Czech Technical University in Prague, Faculty of Nuclear Sciences and Physical Engineering (FNSPE), Břehová 7, 11519 Prague, Czech Republic; michal.krelina@cvut.cz

* Correspondence: boris.kopeliovich@usm.cl

Abstract: We made the first attempt to understand the observed unusual t dependence of single-spin asymmetry observed in the HJET experiment at RHIC. Usually, the interaction of hadrons is presented as a long-range Coulomb interaction and a short-range strong interaction with Coulomb corrections. Such a division gives rise to a Coulomb phase of the hadronic term. Conversely, here we consider short-range hadronic interaction as a correction to the long-range electromagnetic term, i.e., we treat it as an absorptive correction. This significantly affects the Coulomb-nuclear interference, which is a source of single-spin azimuthal asymmetry at small angles.

Keywords: single-spin asymmetry; Coulomb-nuclear interference; Pomeron spin

1. Introduction

Elastic scattering is usually characterized by spin non-flip f_{nf} and spin-flip f_{sf} amplitudes, which determine the differential elastic cross-sections and single-spin azimuthal asymmetry $A_N(t)$,

$$\frac{d\sigma_{el}}{dt} = \pi(|f_{nf}|^2 + |f_{sf}|^2), \quad (1)$$

$$A_N \frac{d\sigma_{el}}{dt} = -2\pi \operatorname{Im}(f_{nf}f_{sf}^*), \quad (2)$$

where t is 4-momentum transfer squared. The latter contains interference of the helicity amplitudes, which makes polarization effects sensitive to the hadron interaction dynamics [1,2].

According to Equation (2), an important condition for azimuthal asymmetry is the existence of a phase shift between the spin amplitudes. However, to the best of our knowledge, the phases of f_{nf} and f_{sf} at high energies are similar. For example, in the Regge pole model, f_{sf}^h and f_{nf}^h have the same phase given by the signature factor. To maximize $A_N(t)$, one should combine hadronic and electromagnetic amplitudes [3]. While the former is predominantly imaginary, the latter is nearly real. Apparently, a sizable effect is expected at small momentum transfer squared t , where the Coulomb and hadronic amplitudes are of the same order. The t dependence of asymmetry in pp scattering is described in a simplified approximation [3] by

$$A_N^{pp}(t) = A_N^{pp}(t_p) \frac{4y^{3/2}}{3y^2 + 1}, \quad (3)$$



Citation: Kopeliovich, B.; Krelina, M.; Potashnikova, I. Coulomb-Nuclear Interference in Polarized pA Scattering. *Universe* **2024**, *1*, 0. <https://doi.org/>

Received:

Accepted:

Published:



Copyright: © 2024 by the authors. Licensee MDPI, Basel, Switzerland. This article is an open access article distributed under the terms and conditions of the Creative Commons Attribution (CC BY) license (<https://creativecommons.org/licenses/by/4.0/>).

where $y = -t/t_p^{pp}$ and

$$t_p^{pp} = \frac{8\sqrt{3}\pi\alpha_{em}}{\sigma_{tot}^{pp}}; \quad (4)$$

$$A_N^{pp}(t_p) = \frac{\sqrt{3}t_p}{4m_p}(\mu_p - 1). \quad (5)$$

Here, $\alpha_{em} = 1/137$ is the fine structure constant; $\mu_p = 2.79$ is the proton magnetic moment. The asymmetry $A_N^{pp}(t)$ reaches a maximum (5) of about 4–5%, at $t = t_p \approx 2 \times 10^{-3} \text{ GeV}^2$. For the sake of simplicity, we assume here, like in [3], a pure non-flip and imaginary hadronic amplitude, no Coulomb phase, etc. In what follows, we present most of these simplifications.

The CNI asymmetry Equation (3) predicted in [3] was confirmed by measurements in [4,5]. It is worth mentioning at least two important practical applications of the CNI effect. First, it is a unique opportunity to measure the spin-flip component of the hadronic amplitude at high energies [6,7].

Second, an important application of CNI-generated azimuthal asymmetry is the possibility to measure the polarization of the beam, in particular at RHIC. The usage of CNI as a polarimeter has been intensively studied in [8–21].

Similar relations can be applied to proton–nucleus elastic scattering,

$$t_p^{pA} = K_A t_p^{pp}, \quad (6)$$

with

$$K_A = \frac{Z\sigma_{tot}^{pp}}{\sigma_{tot}^{pA}}. \quad (7)$$

Correspondingly, the maximal value of A_N at $t = t_p^{pA}$ reads,

$$A_N^{pA}(t_p^{pA}) = \sqrt{K_A} A_N^{pp}(t_p). \quad (8)$$

A simple estimate $\sigma_{tot}^{pA} \sim A^{2/3}\sigma_{tot}^{pp}$ leads to non-dramatic modification of the CNI asymmetry, with about a 20% increase in $A_N^{pA}(t_p^{pA})$ even for heavy nuclei, e.g., gold.

The energy of 100 GeV in the Lab frame is not sufficiently high to suppress iso-vector Reggeons, which have quite a large (dominating) spin-flip component. This is why it is difficult to disentangle large Reggeon and small Pomeron spin-flip terms. On iso-scalar nuclei, e.g., carbon, copper, etc., iso-vector Reggeons are completely excluded, otherwise they are suppressed by a small factor $(A - 2Z)/A$.

2. Born Approximation

The elastic pA amplitude is fully described by two helicity amplitudes $f_{nf, sf}$ defined in [2], each having hadronic and electromagnetic parts, $f_i(q_T) = f_i^h(q_T) + f_i^{em}(q_T)$, where for small-angle elastic scattering $t \equiv -q^2 \approx -q_T^2$, they are comparable.

Hadronic Born amplitudes can be represented as

$$f_{nf}^{pA(h)}(q_T)|_B = \frac{\sigma_{tot}^{pA}}{4\pi} F_A^h(q_T^2), \quad (9)$$

$$f_{sf}^{pA(h)}(q_T)|_B = r_5^{pA} \frac{q_T}{m_N} \frac{\sigma_{tot}^{pA}}{4\pi} \text{Im} F_A^h(q_T^2), \quad (10)$$

where r_5^{pA} is a nuclear analog of r_5^{pp} defined in [2]

$$r_5^{pp} = \frac{m_N f_{sf}(q_T)}{q_T \text{Im} f_{nf}(q_T)}. \quad (11)$$

For pp elastic scattering, r_5^{pp} was fitted to data in [5,7].

The hadronic nuclear form factor $F_A^h(q_T^2)$ in Equations (9)–(10) can be evaluated within the Glauber approximation [22],

$$F_A^h(q_T) = \frac{2i}{\sigma_{tot}^{pA}} \int d^2b e^{i\vec{q}_T \cdot \vec{b}} \left[1 - \left(1 - \frac{1}{2A} \sigma_{tot}^{pp} (1 - i\rho_{pp}(s)) T_A^h(b) \right)^A \right], \quad (12)$$

as well as the total nuclear cross-section,

$$\sigma_{tot}^{pA} = 2\text{Im} \int d^2b i \left[1 - \left(1 - \frac{1}{2A} \sigma_{tot}^{pp}(s) (1 - i\rho_{pp}(s)) T_A^h(b) \right)^A \right]. \quad (13)$$

Correspondingly, the Born electromagnetic amplitudes read

$$f_{nf}^{pA(em)}(q_T) \Big|_B = -2Z\alpha_{em} \frac{1}{q_T^2 + \lambda^2} F_A^{em}(q_T), \quad (14)$$

$$f_{sf}^{pA(em)}(q_T) \Big|_B = -Z\alpha_{em} \frac{1}{m_N q_T} (\mu_p - 1) F_A^{em}(q_T), \quad (15)$$

where the small fictitious photon mass λ is introduced to avoid infrared divergence. The final results are checked for stability at $\lambda \rightarrow 0$.

The nuclear electromagnetic form factor in Equations (14) and (15) has the form

$$F_A^{em}(q_T) = \frac{1}{Z} \int d^2b e^{i\vec{q}_T \cdot \vec{b}} T_Z(b), \quad (16)$$

The nuclear thickness functions are defined as

$$T_A(b) = \int_{-\infty}^{\infty} dz \rho(b, z), \quad (17)$$

where $\rho(b, z)$ is the nuclear density distribution function, and $T_Z(b) = T_A(b) Z/A$.

Following [22,23], next we replace the nuclear thickness function with a more accurate effective thickness function convoluted with NN elastic amplitude

$$T_A(b) \Rightarrow T_A^h(b), \quad (18)$$

where

$$T_A^h(b) = \frac{2}{\sigma_{tot}^{hN}} \int d^2s \text{Re}\Gamma^{hN}(s) T_A(\vec{b} - \vec{s}); \quad (19)$$

$$\text{Re}\Gamma^{hN}(s) = \frac{\sigma_{tot}^{hN}}{4\pi B_{hN}} \exp\left(-\frac{s^2}{2B_{hN}}\right), \quad (20)$$

where B_{hN} is the slope of the differential hN elastic cross-section. This effective nuclear thickness function can be simplified to

$$\begin{aligned} T_A^h(b) &= \frac{2}{\sigma_{tot}^{hN}} \int d^2s \frac{\sigma_{tot}^{hN}}{4\pi B_{hN}} \exp\left(-\frac{s^2}{2B_{hN}}\right) T_A(\vec{b} - \vec{s}) \\ &= \frac{1}{2\pi B_{hN}} \int ds d\phi s \exp\left(-\frac{s^2}{2B_{hN}}\right) T_A(\sqrt{b^2 + s^2 - 2bs \cos \phi}). \end{aligned} \quad (21)$$

3. Hadronic vs. Electromagnetic Amplitudes

The long-range Coulomb forces affect the strong-interaction amplitude by generating a phase shift, known as the Coulomb phase [24–26]. The interplay of Coulomb and hadronic interaction mechanisms is illustrated in Figure 1, following the consideration of this problem in [24].

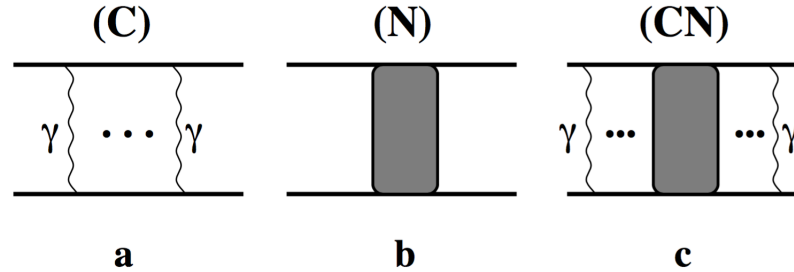


Figure 1. Three types of interaction: pure electromagnetic (a), pure strong interaction (b), and combined strong and electromagnetic interactions (c).

In [24] the last two graphs, (N) and (CN) were combined and treated as a Coulomb-modified strong-interaction amplitude. The modification was approximated by giving an extra phase factor to the hadronic amplitude. In the literature, this factor is called the Coulomb phase [24–26]. Alternatively, one can combine (C) and (CN) and obtain a hadronic correction to the Coulomb amplitude. In what follows, we call this absorptive correction [27,28].

As usual, multiple interaction amplitudes, depicted in Figure 1, are easily calculated in impact parameter representation, where the result is just a product of multiple amplitudes. Thus, we switch from q_T to b dependent amplitudes, and simultaneously, from the Born approximation to the eikonal optical model.

$$\gamma_{nf}^{pA(h)}(b) = \frac{i}{2\pi} \int d^2q_T e^{-i\vec{q}_T \cdot \vec{b}} f_{nf}^{pA(h)}(q_T) \quad (22)$$

$$\gamma_{sf}^{pA(h)}(b) = \frac{i}{2\pi} \int d^2q_T e^{-i\vec{q}_T \cdot \vec{b}} f_{sf}^{pA(h)}(q_T) \quad (23)$$

These hadronic eikonal phases were used in the Glauber model expressions (12) and (13).

Adding higher order terms to the Born Coulomb amplitudes (22) and (23), as is explained in [28], we arrive at the eikonal form for the electromagnetic amplitudes

$$f_{nf}^C(q_T) = \frac{i}{2\pi} \int d^2b e^{i\vec{q}_T \cdot \vec{b}} \left(1 - e^{i\chi_{nf}^C(b)} \right), \quad (24)$$

$$f_{sf}^C(q_T) = \frac{1}{2\pi} \int d^2b e^{i\vec{q}_T \cdot \vec{b}} \chi_C^{sf}(b) e^{i\chi_{nf}^C(b)}, \quad (25)$$

with Coulomb eikonal phases, given by the Born amplitudes in impact parameter representation.

$$\chi_{nf}^C(b) = \frac{-2Z\alpha_{em}}{2\pi} \int d^2q_T e^{-i\vec{q}_T \cdot \vec{b}} \frac{F_A^{em}(q_T)}{q_T^2 + \lambda^2} \quad (26)$$

$$\chi_{sf}^C(b) = \frac{-Z\alpha_{em}(\mu_p - 1)}{2\pi m_N} \int d^2q_T e^{-i\vec{q}_T \cdot \vec{b}} \frac{F_A^{em}(q_T)}{q_T^2 + \lambda^2} \frac{\vec{q}_T \cdot \vec{b}}{b}. \quad (27)$$

Combining the Coulomb (C) with Coulomb-nuclear (CN) mechanisms depicted in Figure 1, one obtains the Coulomb terms, Equations (24) or (25), which acquire an absorption factor, given by the standard Glauber eikonal approximation [29],

$$\begin{aligned} S(b) &= 1 - \gamma_{nf}^{pA(h)}(b) = \left(1 - \frac{1}{2A} \sigma_{tot}^{pp}(s) (1 - i\rho_{pp}(s)) T_A^h(b)\right)^A \\ &\approx \exp\left[-\frac{1}{2} \sigma_{tot}^{pp}(s) T_A^h(b)\right]. \end{aligned} \quad (28)$$

As usual, the complicated multi-loop integrations in momentum representation are essentially simplified to a multiplicative combination in impact parameters. This is why the correction $S(b)$ of Equation (28) enters the final expressions as a factor. Thus, the absorption-corrected amplitudes \tilde{f} take the form

$$\tilde{f}_{nf}^C(q_T) = \frac{i}{2\pi} \int d^2b e^{i\vec{q}_T \cdot \vec{b}} \left(1 - e^{i\chi_{nf}^C(b)}\right) S(b), \quad (29)$$

$$\tilde{f}_{sf}^C(q_T) = \frac{1}{2\pi} \int d^2b e^{i\vec{q}_T \cdot \vec{b}} \chi_C^{sf}(b) e^{i\chi_{nf}^C(b)} S(b), \quad (30)$$

Eventually, we arrive at the full amplitudes.

$$f_{nf,sf}(q_T) = \tilde{f}_{nf,sf}^C(q_T) + f_{nf,sf}^N(q_T). \quad (31)$$

4. Results vs. Data

Now we are in a position to calculate the proton–nucleus total cross-section and single-spin asymmetry, given by Equations (1)–(2). The results are compared with the data in Figures 2–5.

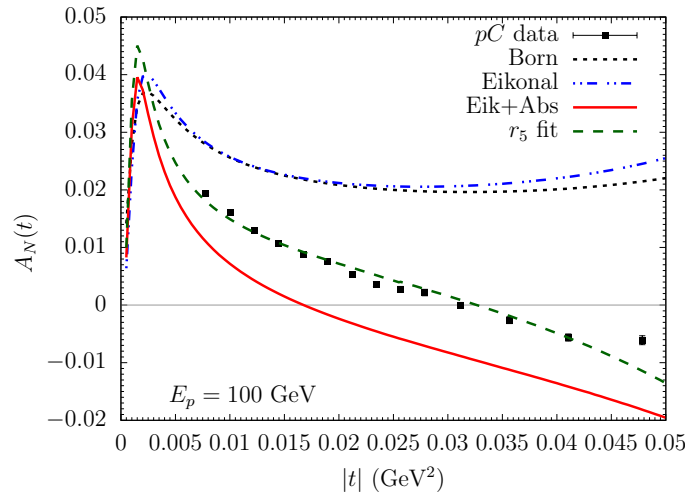


Figure 2. Azimuthal asymmetry in proton–carbon elastic scattering. Black dotted curve presents Born approximation, Equations (9)–(10) and (14)–(15). Double-dot-dashed blue and solid red curves correspond to Eikonal approximation without, (24)–(25), and with, (29)–(30), absorptive corrections, respectively. In both cases, $r_5^{pA} = 0$; data for pC scattering at 100 GeV are from [30].

First of all, we performed calculations within the Born approximation, Equations (9) and (10) and (14) and (15). The hadronic spin-flip component was set to zero. The results are depicted with black dotted curves in Figures 2 and 5. The magnitude of A_N substantially exceeds the data.

Then, we relied on the eikonal form of higher order terms, Equations (24) and (25), keeping $r_5 = 0$. The results are depicted with blue double-dot-dashed curves. The

effect of eikonalization turns out to be rather mild, and the discrepancy with the data remains significant.

The next step is the introduction of absorptive corrections, which significantly reduce the values of $A_N(t)$ as is demonstrated by the red solid curves, calculated with Equations (29) and (30) (r_5 is still zero).

Eventually, we can adjust the single unknown parameter, r_5^{pA} , for each nuclear target. The results of the fit are presented in Table 1.

The found values of r_5^{pA} are pretty close to the values for the Pomeron spin component found by fitting to the pp data in [7].

With values of r_5 in Table 1 and amplitude Equations (29)–(30), we plot the green dashed curves, which we treat as our final results.

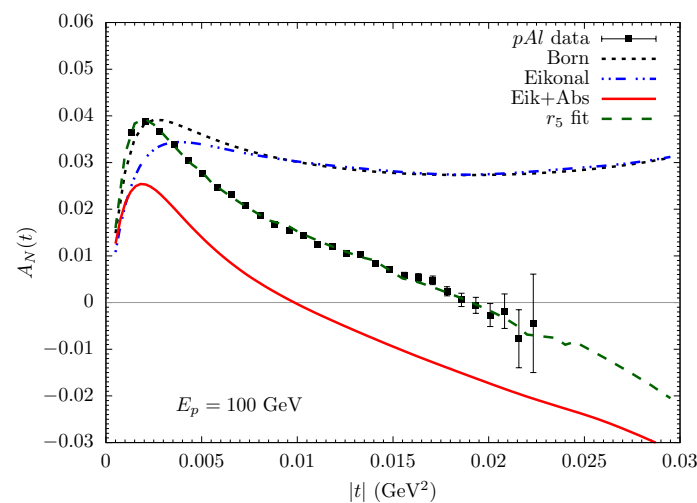


Figure 3. The same as in Figure 2, but for proton–aluminum elastic scattering. Data at 100 GeV are from [31].

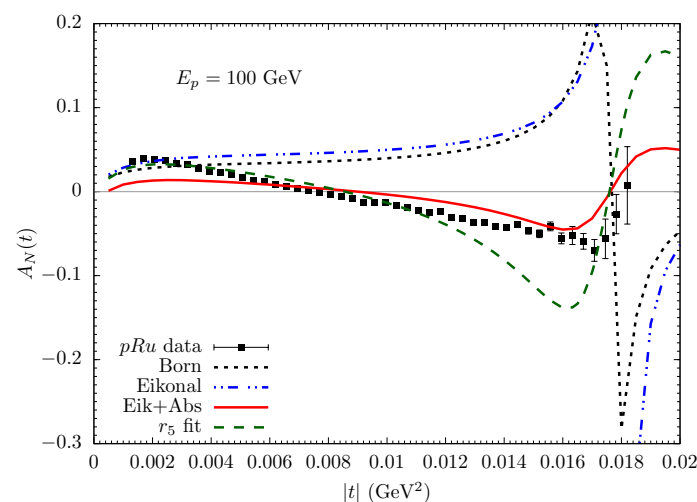


Figure 4. The same as in Figure 2, but for proton–ruthenium elastic scattering. Data at 100 GeV are from [32].

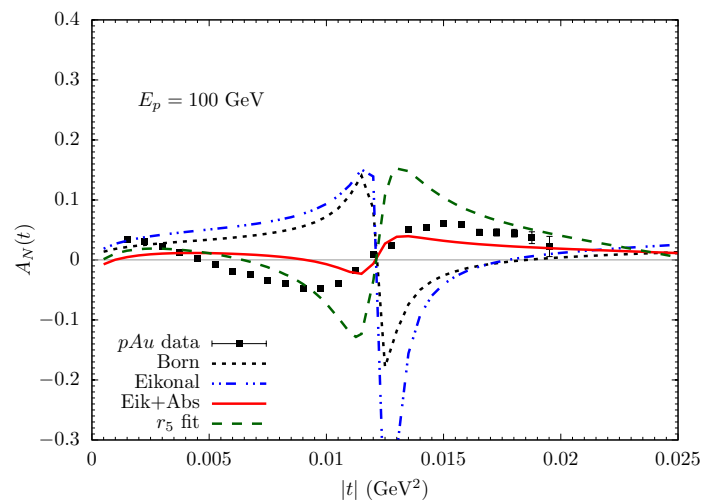


Figure 5. The same as in Figure 2, but for proton–gold elastic scattering. Data at 100 GeV are from [31,32].

Table 1. Results of fit for r_5^{pA} to data on $A_N(t)$ for different nuclei [30–32].

Experiment	Re r_5 fit	Im r_5 fit
p-C @ 100 GeV	-0.071 ± 0.003	-0.063 ± 0.005
p-Al @ 100 GeV	-0.080 ± 0.001	-0.101 ± 0.002
p-Ru @ 100 GeV	-0.068 ± 0.001	-0.469 ± 0.002
p-Au @ 100 GeV	-0.027 ± 0.008	-0.526 ± 0.006

Notice that the nuclear data are quite sensitive to the value of r_5^{pA} ; this is why the CNI method was proposed [6] as a unique way for measuring the hadronic spin-flip amplitudes at high energies.

5. Conclusions

Concluding, we performed the first calculation of single-spin asymmetry in polarized proton–nucleus elastic scattering in the CNI region. We achieved a reasonable agreement with the data, in spite of the rather complicated theoretical construction. The remarkable feature of the nuclear form factor (12) is a change in the sign of the imaginary part of the elastic hadronic non-flip amplitude corresponding to the first zero of the Bessel function $J_1(t)$. Since the non-flip hadronic amplitude significantly exceeds the spin-flip part, they become of the same order right before and after the former changes sign. The asymmetry $A_N(t)$ Equation (2) reaches maximum at $f_{nf} = f_{sf}$, so $A_N(t)$ should abruptly vary between positive and negative maxima in the vicinity of the Bessel zero. Comparison with the data in Figures 4 and 5 confirms such behavior; indeed, the measured $A_N(t)$ exposes two maxima with opposite signs with positions close to predicted.

However, the magnitude of these maxima is exaggerated in our calculations, so there is still room for improvements. Here, nuclear effects were evaluated within the Glauber approximation, which is subject to Gribov inelastic shadowing corrections [33,34]. Their calculation requires substantial modeling, including knowledge of the proton wave function, interaction mechanism, etc. This needs a detailed study, as was performed in [23]. We leave this issue for future development.

Funding: This work was supported in part by grants ANID—Chile FONDECYT 1231062, ANID PIA/APOYO AFB220004, and ANID—Millennium Science Initiative Program ICN2019_044.

References

1. Bilen'ky, S.M.; Lapidus, L.I.; Ryndin, M. R. Polarized proton target in experiments with high-energy particles. *Sov. Phys. Usp.* **1965**, *7*, 721. [*Usp. Fiz. Nauk* **1964**, *84* 243].
2. Buttimore, N.H.; Kopeliovich, B.Z.; Leader, E.; Soffer, J.; Trueman, T.L. The spin dependence of high-energy proton scattering. *Phys. Rev. D* **1999**, *59*, 114010.
3. Kopeliovich, B.Z.; Lapidus, L.I. 'On the necessity of polarization experiments in colliding p p and anti-p p beams. *Yad. Fiz.* **1974**, *19*, 218.
4. Akchurin, N.; Langland, J.; Onel, Y.; Bonner, B.E.; Corcoran, M.D.; Cranshaw, J.; Nessi-Tedaldi, F.; Nessi, M.; Nguyen, C.; Roberts, J.B.; Skeens, J. [E581/704 Collaboration] Analyzing power measurement of p p elastic scattering in the Coulomb—nuclear interference region with the 200-GeV/c polarized proton beam at Fermilab. *Phys. Rev. D* **1993**, *48*, 3026.
5. Poblaguev, Zelenski, A.A.; Aschenauer, A.; Atoian, E.; Eyser, G.; Huang, K.O.; Makdisi, H.; Schmidke, Y.; Alekseev, W.B.; Svirida, I.; et al. Precision Small Scattering Angle Measurements of Elastic Proton-Proton Single and Double Spin Analyzing Powers at the RHIC Hydrogen Jet Polarimeter. *Phys. Rev. Lett.* **2019**, *123*, 162001.
6. Kopeliovich, B.Z.; Zakharov, B.G. Spin-Flip Component of the Pomeron. *Phys. Lett. B* **1989**, *226*, 156.
7. Kopeliovich, B.Z.; Krelina, M.; Potashnikova, I.K. Probing the Pomeron spin structure with Coulomb-nuclear interference. *Phys. Lett. B* **2021**, *816*, 136262.
8. Poblaguev, A.A.; Atoian, G.; Buttimore, N.H.; Zelenski, A. On the Possibility of Measuring the Polarization of a ^3He Beam at EIC by the HJET Polarimeter. *JPS Conf. Proc.* **2022**, *37*, 021103. <https://doi.org/10.7566/JPSCP.37.021103>.
9. Poblaguev, A.A.; Zelenski, A.; Aschenauer, E.; Atoian, G.; Eyser, K.O.; Huang, H.; Schmidke, W.B.; Alekseev, I.; Svirida, D.; Buttimore, N.H. Precision small scattering angle measurements of proton-proton and proton-nucleus analyzing powers at the RHIC hydrogen jet polarimeter. *arXiv* **2022**, arXiv:2211.17146.
10. Khalek, R.A.; Accardi, A.; Adam, J.; Adamiak, D.; Akers, W.; Albaladejo, M.; Al-bataineh, A.; Alexeev, M.G.; Ameli, F.; Antonioli, P.; et al. Science Requirements and Detector Concepts for the Electron-Ion Collider: EIC Yellow Report. *Nucl. Phys. A* **2022**, *1026*, 122447. <https://doi.org/10.1016/j.nuclphysa.2022.122447>.
11. Poblaguev, A.A.; Zelenski, A.; Aschenauer, E.; Atoian, G.; Eyser, K.O.; Huang, H.; Makdisi, Y.; Schmidke, W.B.; Alekseev, I.; Svirida, D.; et al. Precision Small Scattering Angle Measurements of Elastic Proton-Proton Single and Double Spin Analyzing Powers at the RHIC Hydrogen Jet Polarimeter. *Phys. Rev. Lett.* **2019**, *123*, 162001. <https://doi.org/10.1103/PhysRevLett.123.162001>.
12. Poblaguev, A.; Zelenski, A.; Atoian, G.; Aschenauer, E.C.; Eyser, K.O.; Huang, H.C.; Makdisi, Y.; Schmidke, W.; Alekseev, I.; Svirida, D.; et al. Study of elastic proton-proton single and double spin analyzing powers at RHIC HJET polarimeter. In Proceedings of the SPIN2018, Ferrara, Italy, 9–14 September 2018; volume 143. <https://doi.org/10.22323/1.346.0143>.
13. Buttimore, N.H. A Helium—3 polarimeter using electromagnetic interference. In Proceedings of the PSTP2013 PoS, Charlottesville, VA, USA, September 9–13 2013; volume 057. <https://doi.org/10.22323/1.182.0057>.
14. Buttimore, N.H. Polarizing helium-3 for down quark spin enrichment. *AIP Conf. Proc.* **2013**, *1523*, 231–234. <https://doi.org/10.1063/1.4802156>.
15. Buttimore, N.H. Forward collisions and spin effects in evaluating amplitudes. *AIP Conf. Proc.* **2011**, *1350*, 313–316. <https://doi.org/10.1063/1.3601429>.
16. Akchurin, N.; Buttimore, N.H.; Penzo, A. Spin effects in forward high energy proton scattering. *J. Phys. Conf. Ser.* **2011**, *295*, 012101. <https://doi.org/10.1088/1742-6596/295/1/012101>.
17. Buttimore, N.H. Overview of processes involved in spin transfer collisions. *AIP Conf. Proc.* **2008**, *1008*, 14–23. <https://doi.org/10.1063/1.2932261>.
18. Buttimore, N.H.; O'Brien, D.S. Dynamics of polarization buildup by spin filtering. *Eur. Phys. J. A* **2008**, *35*, 47–55. <https://doi.org/10.1140/epja/i2007-10531-2>.
19. Buttimore, N.H. Asymmetry and peripheral spin dependence. *AIP Conf. Proc.* **2007**, *915*, 685–688. <https://doi.org/10.1063/1.2750872>.
20. Buttimore, N.H.; Leader, E.; Trueman, T.L. An Absolute polarimeter for high-energy protons. *Phys. Rev. D* **2001**, *64*, 094021. <https://doi.org/10.1103/PhysRevD.64.094021>.
21. Bates, A.T.; Buttimore, N.H. Bounds in proton proton elastic scattering at low momentum transfer. *Phys. Rev. D* **2002**, *65*, 014015. <https://doi.org/10.1103/PhysRevD.65.014015>.
22. Kopeliovich, B.Z. Transparent nuclei and deuteron gold collisions at RHIC. *Phys. Rev. C* **2003**, *68*, 044906.
23. Kopeliovich, B.Z.; Potashnikova, I.K.; Schmidt, I. Large rapidity gap processes in proton-nucleus collisions. *Phys. Rev. C* **2006**, *73*, 034901.
24. Kopeliovich, B.Z.; Tarasov, A.V. The Coulomb phase revisited. *Phys. Lett. B* **2001**, *497*, 44–48.
25. Bethe, H.A. Scattering and polarization of protons by nuclei. *Ann. Phys.* **1958**, *3*, 190–240.
26. Cahn, R.N. Coulombic-hadronic interference in an eikonal model. *Z. Phys. C* **1982**, *15*, 253–260.
27. Kopeliovich, B.Z.; Trueman, T.L. Polarized proton nucleus scattering. *Phys. Rev. D* **2001**, *64*, 034004.
28. Kopeliovich, B.Z. High-energy polarimetry at RHIC. *arXiv* **1998**, arXiv:hep-ph/9801414.
29. Glauber, R.J.; Matthiae, G. High-energy scattering of protons by nuclei. *Nucl. Phys. B* **1970**, *21*, 135–157.
30. Jinnouchi, O.; Alekseev, I.G.; Bravar, A.; Bunce, G.; Dhawan, S.; Huang, H.; Igo, G.; Kanavets, V.P.; Kurita, K.; Okada, H.; et al. Measurement of the analyzing power of proton-carbon elastic scattering in the CNI region at RHIC. *arXiv* **2005**, arXiv:nucl-ex/0412053.

31. Poblaguev, A. New DAQ for the HJET polarimeter at RHIC. In Proceedings of the PSTP2015, PoS, Bochum, Germany, 14–18 September 2015; volume 032.
32. Poblaguev, A. Precision small scattering angle measurements of proton-proton and proton- nucleus analyzing powers at the RHIC hydrogen jet polarimeter. *Acta Phys. Pol. Proc.* **2023**, *1* (Suppl. 16), 5.
33. Gribov, V.N. Glauber Corrections And The Interaction Between High-Energy Hadrons And Nuclei. *Sov. Phys. JETP* **1969**, *29*, 483. [*Zh. Eksp. Teor. Fiz.* **1969**, *56*, 892].
34. Kopeliovich, B.Z. Gribov inelastic shadowing in the dipole representation. *Int. J. Mod. Phys. A* **2016**, *31*, 1645021.

Disclaimer/Publisher’s Note: The statements, opinions and data contained in all publications are solely those of the individual author(s) and contributor(s) and not of MDPI and/or the editor(s). MDPI and/or the editor(s) disclaim responsibility for any injury to people or property resulting from any ideas, methods, instructions or products referred to in the content.